CHIN. PHYS. LETT. Vol. 37, No. 7 (2020) 076301

Theoretical Simulation of the Temporal Behavior of Bragg Diffraction Derived from Lattice Deformation

Cong Guo(过聪)[1,2], Shuai-Shuai Sun(孙帅帅)[2], Lin-Lin Wei(尉琳琳)[2], Huan-Fang Tian(田焕芳)[2], Huai-Xin Yang(杨槐馨)[2,3], Shu Gao(高舒)[1], Yuan Tan(谭媛)[1], and Jian-Qi Li(李建奇)[2,3,4*]

[1]*School of Physics and Information Engineering & Key Laboratory of Optoelectronic Chemical Materials and Devices of Ministry of Education, Jianghan University, Wuhan 430056, China*

[2]*Beijing National Laboratory for Condensed Matter Physics, and Institute of Physics, Chinese Academy of Sciences, Beijing 100190, China*

[3]*School of Physical Sciences, University of Chinese Academy of Sciences, Beijing 100049, China*

[4]*Collaborative Innovation Center of Quantum Matter, Beijing 100190, China*

(Received 15 April 2020; accepted 27 May 2020; published online 21 June 2020)

A theoretical study on the structural dynamics of the temporal behavior of Bragg diffraction is presented and compared with experimental results obtained via ultrafast electron crystallography. In order to describe the time-dependent lattices and calculate the Bragg diffraction intensity, we introduce the basic vector offset matrix, which can be used to quantify the shortening, lengthening and rotation of the three lattice vectors (i.e., lattice deformation). Extensive simulations are performed to evaluate the four-dimensional electron crystallography model. The results elucidate the connection between structural deformations and changes in diffraction peaks, and sheds light on the quantitative analysis and comprehensive understanding of the structural dynamics.

PACS: 63.10.+a, 61.05.jd, 42.65.Re DOI: 10.1088/0256-307X/37/7/076301

Recent developments in ultrafast electron diffraction (UED) and ultrafast electron microscopy (UEM) have provided the means to study structural dynamics with space and time resolutions that allow direct observation of transformations affecting the fundamental properties of materials.[1–6] The systems investigated thus far include metallic and semiconducting materials.[7–9] In all of the studies reported so far, a general behavior has been found, namely, temporal changes in the position of Bragg spots (or diffraction rings) and similar changes in diffraction intensities. The temporal behavior of Bragg diffraction has been directly derived from structural dynamics, such as large-amplitude expansions of the lattice structure caused by femtosecond laser excitations and breathing mode oscillations due to coherent acoustic phonon motion.

The following important questions remain unanswered. What occurs during these phenomena at the atomic scale? What is the connection between dynamical structural characteristics and diffraction patterns? How can researchers understand and simulate the temporal changes in Bragg spots, including changes in position and intensity? Hence, a microscopic-level theory is necessary for further investigation of the atomic-scale motions. Such a model may also be important for the elucidation of laser-induced melting and ablation[10–12] and acoustic-wave generation[13–20] and for studies involving transient optical reflectivity,[21,22] time-resolved x-ray diffraction,[23–29] and transmission electron diffraction of metals.[30,31]

In this letter, we present a theoretical study on the temporal behavior of Bragg diffraction. Using a four-dimensional (4D) electron crystallography model, we investigate the influences of lattice deformation on the time dependence of Bragg diffraction intensity. Then, simulations are performed to evaluate the 4D electron crystallography model, and a comparison with experimental results is presented.

In this letter, first 4D electron crystallography and our model for crystal structural transitions are described, together with the needed diffraction intensity expressions for UED. Then, the methodology and results of numerical simulations are presented. Moreover, discussions on the importance of different parameters and their association with real systems are also provided.

To analyze instantaneous atomic configurations during dynamic processes, we extend traditional electron crystallography by introducing a time parameter and developed preliminary theories of 4D electron crystallography.

As the most important step, to describe the time-

Supported by the National Key Research and Development Program of China under Grant Nos. 2016YFA0300303, 2017YFA0504703, and 2017YFA0302904, the National Basic Research Program of China under Grant No. 2015CB921304, the National Natural Science Foundation of China under Grant Nos. 11604372, 11474323, 11774391, 11774403, and 61575085, the Strategic Priority Research Program (B) of the Chinese Academy of Sciences under Grant No. XDB25000000, and the Scientific Instrument Developing Project of the Chinese Academy of Sciences under Grant No. ZDKYYQ20170002.

*Corresponding author. Email: ljq@iphy.ac.cn

© 2020 Chinese Physical Society and IOP Publishing Ltd

dependent lattices, we introduce the basic vector offset matrix $\boldsymbol{C}(t)$:

$$\begin{pmatrix} \boldsymbol{a}(t) \\ \boldsymbol{b}(t) \\ \boldsymbol{c}(t) \end{pmatrix} = \boldsymbol{C}(t) \begin{pmatrix} \boldsymbol{a} \\ \boldsymbol{b} \\ \boldsymbol{c} \end{pmatrix} = \begin{pmatrix} C_{11}(t) & C_{12}(t) & C_{13}(t) \\ C_{21}(t) & C_{22}(t) & C_{23}(t) \\ C_{31}(t) & C_{32}(t) & C_{33}(t) \end{pmatrix} \begin{pmatrix} \boldsymbol{a} \\ \boldsymbol{b} \\ \boldsymbol{c} \end{pmatrix}, \quad (1)$$

where $\boldsymbol{a}(t)$, $\boldsymbol{b}(t)$ and $\boldsymbol{c}(t)$ are the time-dependent lattice basis vectors, while $\boldsymbol{a}$, $\boldsymbol{b}$ and $\boldsymbol{c}$ are the initial lattice basis vectors. This matrix $\boldsymbol{C}(t)$ can be used to quantify the shortening, lengthening and rotation of the three lattice vectors (i.e., lattice deformation). Then, the base vectors of the reciprocal lattices, $\boldsymbol{a}^*(t)$, $\boldsymbol{b}^*(t)$ and $\boldsymbol{c}^*(t)$, can be expressed as

$$\begin{aligned} \boldsymbol{a}^*(t) &= \frac{\boldsymbol{b}(t) \times \boldsymbol{c}(t)}{\boldsymbol{a}(t) \cdot [\boldsymbol{b}(t) \times \boldsymbol{c}(t)]}, \\ \boldsymbol{b}^*(t) &= \frac{\boldsymbol{c}(t) \times \boldsymbol{a}(t)}{\boldsymbol{b}(t) \cdot [\boldsymbol{c}(t) \times \boldsymbol{a}(t)]}, \\ \boldsymbol{c}^*(t) &= \frac{\boldsymbol{a}(t) \times \boldsymbol{b}(t)}{\boldsymbol{c}(t) \cdot [\boldsymbol{a}(t) \times \boldsymbol{b}(t)]}. \end{aligned} \quad (2)$$

For a Bragg spot (hkl), the corresponding reciprocal vector $g_{hkl}(t)$ is

$$\boldsymbol{g}_{hkl}(t) = h\boldsymbol{a}^*(t) + k\boldsymbol{b}^*(t) + l\boldsymbol{c}^*(t). \quad (3)$$

Naturally, we can obtain a very useful parameter, the reciprocal vector offset $\Delta\boldsymbol{g}$,

$$\Delta\boldsymbol{g} = \boldsymbol{g}_{hkl}(t) - \boldsymbol{g}_{hkl}, \quad (4)$$

where $\boldsymbol{g}_{hkl}$ is the initial reciprocal vector.

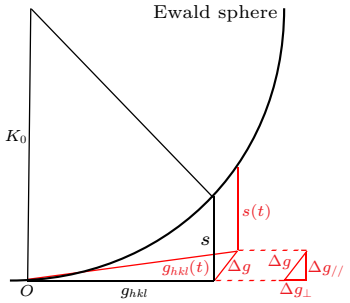

Fig. 1. Schematic diagram showing the reciprocal vector offset $\Delta\boldsymbol{g}$. $\Delta\boldsymbol{g}_{||}$ and $\Delta\boldsymbol{g}_{\perp}$, as components of $\Delta\boldsymbol{g}$, are parallel and perpendicular to the electron wave vector $\boldsymbol{K}_0$, respectively.

Figure 1 shows the reciprocal vector offset $\Delta\boldsymbol{g}$ with $\Delta\boldsymbol{g}_{||}$ and $\Delta\boldsymbol{g}_{\perp}$, as components of $\Delta\boldsymbol{g}$, are parallel and perpendicular to the electron wave vector $\boldsymbol{K}_0$, respectively. Notably, the Ewald sphere is so large that its circumference can be regarded as a horizontal line near O. Changes in the deviation parameter s are primarily due to $\Delta\boldsymbol{g}_{||}$, which has a strong effect on the diffraction intensity. In contrast, temporal changes in the Bragg spot positions are derived from $\Delta\boldsymbol{g}_{\perp}$, and the position of a Bragg spot is described by $\boldsymbol{g}_{hkl}(t)$.

In this study, the intensities of the Bragg spots are expressed as[32,33]

$$I_{\mathrm{g}} = \frac{\sin^2\left(\pi L\sqrt{s^2 + \xi_{\mathrm{g}}^{-2}}\right)}{\xi_{\mathrm{g}}^2(s^2 + \xi_{\mathrm{g}}^{-2})}, \quad (5)$$

where I_{g} represents the Bragg peak intensity, L is the thickness of the crystal, ξ_{g} is the extinction distance, and s is a parameter related to the deviation from the exact Bragg condition. It is worth mentioning that all of the parameters are time-dependent and are functions of $\boldsymbol{a}(t)$, $\boldsymbol{b}(t)$ and $\boldsymbol{c}(t)$, which correspond to the current crystal. For more detail, we have

$$L(t) = L_0 \frac{\left| (\,u \quad v \quad w\,) \begin{pmatrix} \boldsymbol{a} \\ \boldsymbol{b} \\ \boldsymbol{c} \end{pmatrix} \right|}{\left| (\,u \quad v \quad w\,) \begin{pmatrix} \boldsymbol{a}(t) \\ \boldsymbol{b}(t) \\ \boldsymbol{c}(t) \end{pmatrix} \right|}, \quad (6)$$

$$s(t) = |\boldsymbol{K}_0| - \sqrt{|\boldsymbol{K}_0|^2 - |\boldsymbol{g}_{hkl}(t)|^2 + |\Delta\boldsymbol{g}_{||}|^2} - |\Delta\boldsymbol{g}_{||}|, \quad (7)$$

$$\xi_{\mathrm{g}}(t) = \frac{\pi V_c(t)}{\lambda F_{\mathrm{g}}} = \frac{\pi \boldsymbol{a}(t) \cdot [\boldsymbol{b}(t) \times \boldsymbol{c}(t)]}{\lambda F_{\mathrm{g}}}. \quad (8)$$

Formulae (6)–(8) present the parameters L, ξ_{g}, s, which are time-dependent. In these formulae, L_0 is the initial thickness of the crystal, $[u\ v\ w]$ is the zone axis index, $V_c(t)$ is the cell volume, λ is the electron wavelength, and F_{g} is the structure factor.

Formula (5) is a dynamical approximation based on the two-beam dynamical diffraction theory under the assumption of no absorption, in which the interactions among diffracted beams are ignored. Therefore, in this study, only two special cases are discussed. These are the cases of high symmetry in the diffraction pattern for which members of sets of beams are equivalent in that they have equal excitation errors and interact through equivalent structure factor values. The way in which such sets of equivalent beams may be merged gives, for each set, a single representative beam, so that the formula (5) can be used.[32] Furthermore, an extensive theoretical analysis of multi-beam dynamical diffraction is in progress. It is worth noting that, if we take the Debye–Waller effect into consideration, formula (5) would be extended to[34]

$$I_{\mathrm{g}} = \frac{\sin^2\left(\pi L\sqrt{s^2+\xi_{\mathrm{g}}^{-2}}\right)}{\xi_{\mathrm{g}}^2(s^2 + \xi_{\mathrm{g}}^{-2})}\left[(1-\beta)+\beta\exp\left(-\frac{t}{\tau_{\mathrm{e-ph}}}\right)\right], \quad (9)$$

where β is the diffraction intensity decrease caused by the Debye–Waller effect, and $\tau_{\mathrm{e-ph}}$ is the time constant of lattice thermalization associated with electron-phonon coupling.

Next, we give numerical simulations and discussion. To illustrate our model, we present two typical examples based on the excitation of coherent acoustic phonons in nanometer-scale silicon and graphite films. The basic vector offset matrix $\boldsymbol{C}(t)$ can be easily described in these systems. Numerical simulations are performed using the MATLAB code.

Park *et al.* gave a detailed account of the UEM studies of graphite single crystals and observed coherent resonance modulations in graphite diffraction results and images.[7] Details regarding temporal changes in the intensity integral and separation of the graphite $(\bar{1}1\bar{1})$ Bragg spot can be found in Ref. [7].

Based on Ref. [7], the acceleration voltage is 200 keV, and the sample thickness is 392 Å. The basic vector offset matrix $\boldsymbol{C}(t)$ can be described as

$$\boldsymbol{C}(t) = \begin{pmatrix} 1 & 0 & 0 \\ 0 & 1 & 0 \\ 0 & 0 & 1.001 - 0.001\cos(\frac{2\pi t}{20.65}) \end{pmatrix}. \quad (10)$$

Here we use $C_{33} = 1.001 - 0001\cos(\frac{2\pi t}{20.65})$ to indicate a breathing mode oscillation in the $\boldsymbol{c}$ direction. The amplitude has been set to 1‰ of c, and the period is 20.65 ps.

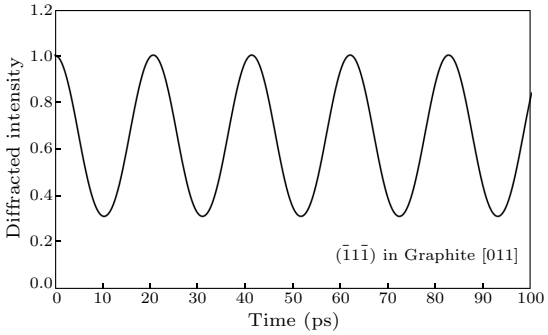

Fig. 2. Numerical simulation results for the diffraction intensity of the $(\bar{1}1\bar{1})$ Bragg spot for graphite along the [011] direction.

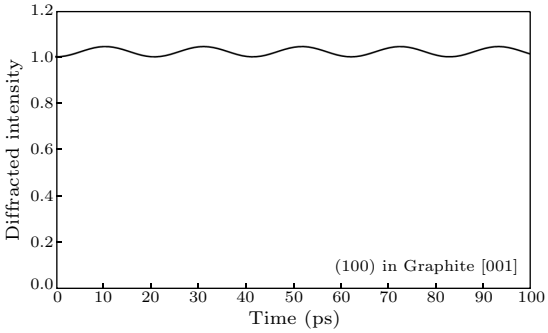

Fig. 3. Numerical simulation results for the diffraction intensity of (100) in graphite along the [001] direction.

In Fig. 2, we present numerical simulation results for the diffraction intensity of the $(\bar{1}1\bar{1})$ Bragg spot for graphite along the [011] direction. Here formula (5) is applied to calculate the Bragg peak intensity and the calculations and simulations are semiquantitative. The intensity shows a substantial change of up to 50%, which agrees with the results in Ref. [7] (the experimental results in the intensity integral of the graphite reported by Park *et al.* are given in Fig. S1 in the Supplementary Materials). Moreover, in Fig. 3, we show the simulation results for the diffraction intensity of (100) in graphite along the [001] direction. As is expected, the intensity shows a change of only 5%, which corresponds to the absence of Bragg spot dynamics reported by Park *et al.*. The temporal behaviors of spot $(\bar{1}1\bar{1})$ and spot (100) are different because the $\Delta \boldsymbol{g}_{||}$ of spot (100) is 0 in ultrafast dynamical processes. The minor change in diffraction intensity for the (100) spot is primarily due to oscillations in the sample thickness L.

We choose silicon as another example because it is a typical semiconductor that has been widely studied. Harb *et al.*[9] reported on the generation and detection of both transverse and longitudinal coherent acoustic phonons in 33-nm free-standing (001)-oriented single-crystalline Si films using femtosecond electron diffraction (FED) to monitor laser-induced atomic displacements. Details regarding temporal changes in the intensity of the silicon (220) Bragg spot can be found in Ref. [9].

Based on Ref. [9], the acceleration voltage is 55 keV, and the sample thickness is 330 Å. The basic vector offset matrix $\boldsymbol{C}(t)$ can be written as

$$\boldsymbol{C}(t) = \begin{pmatrix} C_{11} & 0 & 0 \\ 0 & C_{22} & 0 \\ 0 & 0 & C_{33} \end{pmatrix}. \quad (11)$$

Here we take $C_{11} = 1.001 - 0001\cos(\frac{2\pi t}{11.4})$ and $C_{22} = 1.001 - 0001\cos(\frac{2\pi t}{11.4})$ to indicate a transverse breathing mode. The amplitude has been set to 1‰ of a and 1‰ of b, and the period is 11.4 ps. In addition, we use $C_{33} = 1.003 - 0003\cos(\frac{2\pi t}{7.6})$ to indicate a longitudinal breathing mode. The corresponding amplitude has been set to 3‰ of c, and the period is 7.6 ps. The amplitude is larger in the c direction because c is directed along the free-standing direction and is perpendicular to the film.

In Fig. 4, we present the numerical simulation results for diffraction intensity of the (220) Bragg spot in silicon along the [001] direction. The simulation agrees very well with the experimental data, including the wave phase and amplitude (the experimental data for the diffraction intensity of the silicon reported by Harb *et al.* is illustrated in Fig. S2 in the supplementary material). In this case, the $\Delta g_{||}$ of spot (220) is also 0, while the change in diffraction intensity induced by oscillations in the sample thickness L is large enough to be observed. It should be mentioned that simulations of diffraction spot displacement may be more accurate in principle because they are not mod-

ulated by formulae (5) and (9).

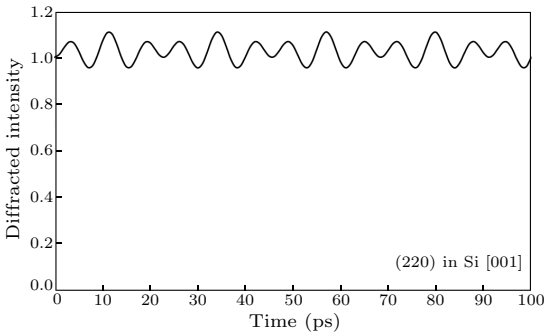

Fig. 4. Numerical simulation results for the diffraction intensity of the (220) Bragg spot in silicon along the [001] direction.

Finally, we note that 4D electron crystallography can contribute to establishing the connection between structural transitions and changes in diffraction peaks. If one knows the details governing structural transitions, the basic vector offset matrix $\boldsymbol{C}(t)$ can be written, and the temporal behavior of diffraction patterns can be simulated. In contrast, if we have data regarding temporal changes in diffraction patterns, we can solve the basic vector offset matrix $\boldsymbol{C}(t)$ and analyze the structural transitions.

In summary, we have reported a theoretical study of structural dynamics for the temporal behavior of Bragg diffraction derived from lattice deformation. In order to describe the time-dependent lattices and calculate the Bragg diffraction intensity, we introduce the basic vector offset matrix, which can be used to quantify the shortening, lengthening and rotation of the three lattice vectors (i.e., lattice deformation). Extensive simulations were performed and compared with the experimental results obtained via ultrafast electron crystallography to evaluate the 4D electron crystallography model. The results elucidate the connection between structural transitions and changes in diffraction peaks. This work sheds light on the quantitative analysis and comprehensive understanding of the structural dynamics.

References

[1] Zewail A H 2006 *Annu. Rev. Phys. Chem.* **57** 65
[2] Tang J, Yang D S and Zewail A H 2007 *J. Phys. Chem. C* **111** 8957
[3] Yang D S, Gedik N and Zewail A H 2007 *J. Phys. Chem. C* **111** 4889
[4] Cao G, Sun S, Li Z, Tian H, Yang H and Li J 2015 *Sci. Rep.* **5** 8404
[5] Greig S R and Elezzabi A Y 2016 *Sci. Rep.* **6** 19056
[6] Mohd Bahar A A, Zakaria Z, Md. Arshad M K, Isa A A M, Dasril Y and Alahnomi R A 2019 *Sci. Rep.* **9** 5467
[7] Park H S, Baskin J S, Barwick B, Kwon O H and Zewail A H 2009 *Ultramicroscopy* **110** 7
[8] Fritz D M *et al.* 2007 *Science* **315** 633
[9] Harb M, Peng W, Sciaini G, Hebeisen C T, Ernstorfer R, Eriksson M A, Lagally M G, Kruglik S G and Miller R D 2009 *Phys. Rev. B* **79** 094301
[10] Jiang L and Tsai H L 2005 *J. Heat. Trans.* **127** 1167
[11] Bechtel J H 1975 *J. Appl. Phys.* **46** 1585
[12] Wellershoff S S, Hohlfeld J, Güdde J and Matthias E 1999 *Appl. Phys. A* **69** S99
[13] Wright O B and Kawashima K 1992 *Phys. Rev. Lett.* **69** 1668
[14] Rossignol C, Rampnoux J M, Perton M, Audoin B and Dilhaire S 2005 *Phys. Rev. Lett.* **94** 166106
[15] Wright O B 1994 *Phys. Rev. B* **49** 9985
[16] Hase M, Ishioka K, Demsar J, Ushida K and Kitajima M 2005 *Phys. Rev. B* **71** 184301
[17] Hartland G V 2004 *Phys. Chem. Chem. Phys.* **6** 5263
[18] Thomsen C, Grahn H T, Maris H J and Tauc J 1986 *Phys. Rev. B* **34** 4129
[19] Hodak J H, Henglein A and Hartland G V 2000 *J. Phys. Chem. B* **104** 5053
[20] Eesley G L, Clemens B M and Paddock C A 1987 *Appl. Phys. Lett.* **50** 717
[21] Brorson S D, Fujimoto J G and Ippen E P 1987 *Phys. Rev. Lett.* **59** 1962
[22] Sun C, Vallée F, Acioli L, Ippen E P and Fujimoto J G 1993 *Phys. Rev. B* **48** 12365
[23] Lindenberg A M *et al.* 2000 *Phys. Rev. Lett.* **84** 111
[24] Cavalleri A *et al.* 2000 *Phys. Rev. Lett.* **85** 586
[25] Rose-Petruck C *et al.* 1999 *Nature* **398** 310
[26] Decamp M F, Reis D A, Fritz D M, Bucksbaum P H, Dufresne E M and Clarke R 2005 *J. Synchrotron Rad.* **12** 177
[27] Plech A *et al.* 2003 *Europhys. Lett.* **61** 762
[28] Fan H and Pan X 1998 *Chin. Phys. Lett.* **15** 547
[29] Guo X, Jiang Z Y, Chen L, Chen L, Xin J, Rentzepis P M and Chen J 2015 *Chin. Phys. B* **24** 108701
[30] Nie S, Wang X, Park H, Clinite R and Cao J 2006 *Phys. Rev. Lett.* **96** 025901
[31] Park H, Wang X, Nie S, Clinite R and Cao J 2005 *Phys. Rev. B* **72** 100301
[32] Cowley J M 1995 *Diffraction Physics* (Amsterdam: Elsevier)
[33] Williams D B and Carter C B 1996 *Transmission Electron Microscopy: A Textbook for Materials Science* (New York: Plenum Press)
[34] Wei L *et al.* 2017 *J. Biomol. Struct. Dyn.* **4** 044012

Supplementary Materials: Theoretical Simulation of the Temporal Behavior of Bragg Diffraction Derived from Lattice Deformation*

Cong Guo(过聪), Shuai-Shuai Sun(孙帅帅), Lin-Lin Wei(尉琳琳),

Huan-Fang Tian(田焕芳), Huai-Xin Yang(杨槐馨), Shu Gao(高舒),

Yuan Tan(谭媛), Jian-Qi Li(李建奇)**

*Supported by the National Key Research and Development Program of China under Grant Nos. 2016YFA0300303, 2017YFA0504703, and 2017YFA0302904, the National Basic Research Program of China under Grant No. 2015CB921304, the National Natural Science Foundation of China under Grant Nos. 11604372, 11474323, and 11774391, 11774403 and 61575085, the Strategic Priority Research Program (B) of the Chinese Academy of Sciences under Grant No. XDB25000000, and the Scientific Instrument Developing Project of the Chinese Academy of Sciences under Grant No. ZDKYYQ20170002.

**Corresponding author. Email: ljq@iphy.ac.cn

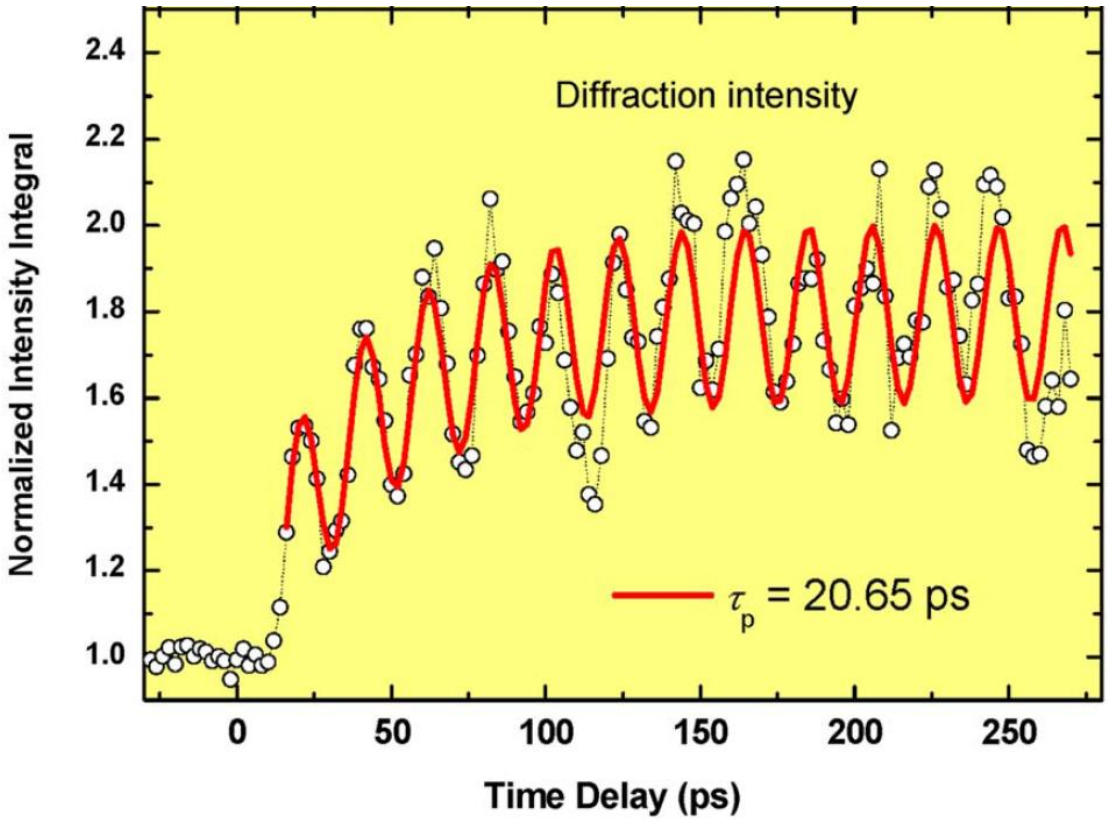

FIG. S1 Resonance dynamics in graphite diffraction. Temporal change in the intensity integral of the graphite $(\bar{1}1\bar{1})$ Bragg spot. [1]

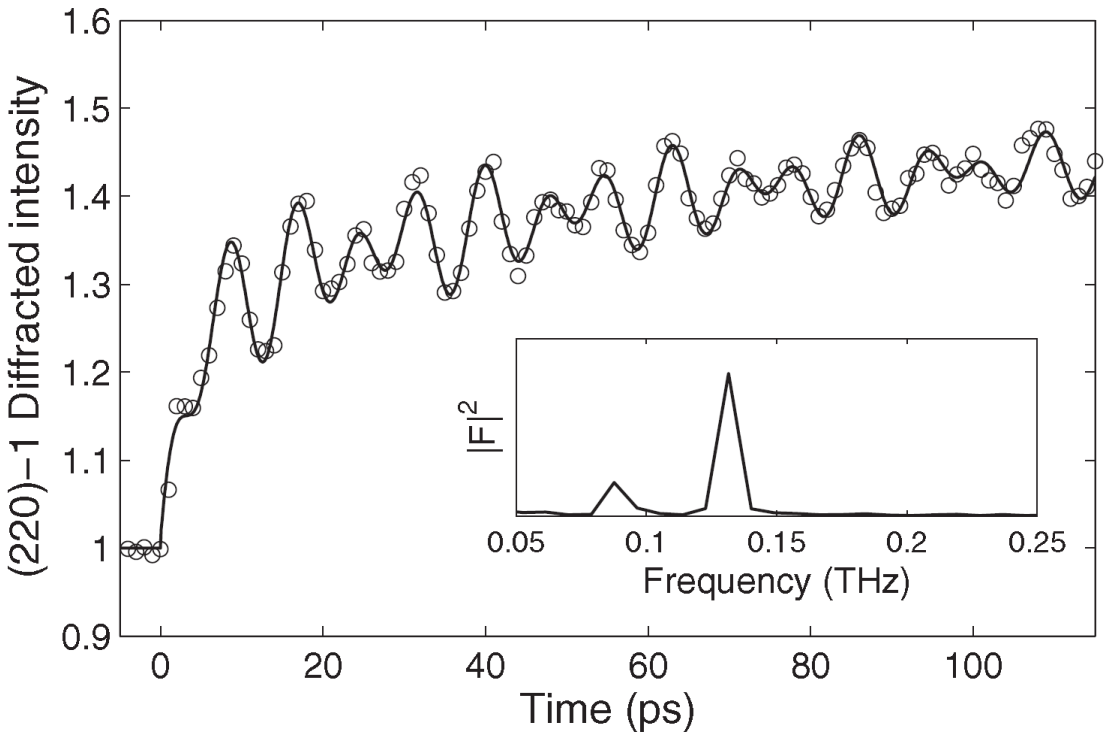

FIG. S2 Kinetics of the (220)-1 spot (circles) along with a fit that includes a biexponential rise component and two damped sinusoidal functions (solid line). [2]

References

[1] Park H. S., Baskin J. S., Barwick B., Kwon O. H., and Zewail A. H., 2009 *Ultramicroscopy* **110** 7

[2] Harb M., Peng W., Sciaini G., Hebeisen C. T., Ernstorfer R., Eriksson M. A., Lagally M. G., Kruglik S. G., and Miller R. D., 2009 *Phys. Rev. B* **79** 094301